Journal of Materials Chemistry B

RSC Publishing

PAPER

View Article Online
View Journal | View Issue

Cite this: J. Mater. Chem. B, 2013, 1, 4601

Doxorubicin-loaded electrospun poly(L-lactic acid)/mesoporous silica nanoparticles composite nanofibers for potential postsurgical cancer treatment

Kexin Qiu,[abc] Chuanglong He,*[ab] Wei Feng,[b] Weizhong Wang,[b] Xiaojun Zhou,[abc] Zhiqi Yin,[b] Liang Chen,[b] Hongsheng Wang[ab] and Xiumei Mo[abc]

Received 2nd May 2013
Accepted 17th July 2013

DOI: 10.1039/c3tb20636j

www.rsc.org/MaterialsB

A drug-loaded implantable scaffold is a promising alternative for the treatment of a tissue defect after tumor resection. In this study, mesoporous silica nanoparticles (MSNs) were used as carriers to load an anticancer drug – doxorubicin hydrochloride (DOX), and the DOX-loaded MSNs (DOX@MSNs) were subsequently incorporated into poly(L-lactic acid) (PLLA) nanofibers *via* electrospinning, resulting in a new drug-loaded nanofibrous scaffold (PLLA/DOX@MSNs). The as-prepared composite nanofibrous scaffold was characterized by various techniques. *In vitro* release profiles of DOX from PLLA/DOX@MSNs composite nanofibers were examined and the *in vitro* antitumor efficacy against HeLa cells was also evaluated. The results showed that DOX-loaded MSNs were successfully incorporated into composite nanofibers with different MSN (or DOX) contents. Among them, the PLLA/1.0% DOX@10% MSN nanofibers exhibited good particle distribution and improved thermal stability. More importantly, they possessed high DOX-loading capacities due to which the drug can be released in a sustained and prolonged manner, and therefore higher *in vitro* antitumor efficacy than their MSNs-free counterparts. Thus, the prepared PLLA/MSNs composite nanofibrous mats are highly promising as local implantable scaffolds for potential postsurgical cancer treatment.

Introduction

Local tumor recurrence remains a major clinical problem following surgical treatment for most cancers such as lung,[1] breast,[2] head and neck,[3] colon,[4] and prostatic malignancies,[5] which is usually caused by inadequate resection or implantation during surgery. Both radiation and chemotherapy are commonly used for adjuvant therapies after surgical resection to reduce the risk of local recurrence, but these therapies frequently result in severe side effects that can affect the patient's quality of life and even kill the patient. Additionally, the immediate repair and reconstruction of tissue defects after tumor resection are of great significance for long-term successful healing in many cancer therapies.[2,4] Thus, it is desirable to develop an implantable local drug delivery scaffold by integrating anticancer drugs into a biodegradable scaffold.

Localized delivery of anticancer drugs directly to the site where there is high risk of tumor recurrence has been proposed as a promising alternative approach for preventing local tumor recurrence after surgery.[6] Generally, local drug delivery can be achieved using various dosage forms including drug-eluting films, hydrogels, wafers, rods, microspheres, and nanoparticles,[7–9] the majority of which are biodegradable polymer-based drug delivery systems so as to avoid a second surgery for implant removal. These systems have been used to decrease local recurrence rates in many cancer types, but so far have met with limited clinical success,[4] which has led to the increasing development of novel drug delivery devices, especially of an implantable drug delivery film. Among them, a drug-loaded nanofibrous scaffold offers significant advantages for synergistic treatment of tissue regeneration and cancer recurrence in tumor defects. While the anticancer drug kills the tumor cells, the nanofibrous scaffold endows a favorable microenvironment for tissue construction of tumor defects, thus contributing a long-term tumor healing.

Electrospun polymer fibers have been extensively used as implantable drug delivery devices with very encouraging preliminary results,[4,5,10,11] due to their unique architectural features and robust drug loading capability. Several anticancer drugs including carmustine,[10] paclitaxel,[5,11] doxorubicin,[12–16] cisplatin,[3] polyphenol,[17] and camptothecin[4] have been loaded into various electrospun fibers for postsurgical cancer treatment. These medicated fiber mats can be fabricated using blend,[11] coaxial,[18] and emulsion electrospinning,[6,13,16] and the drug release from these fiber mats is either diffusion-controlled

[a]State Key Laboratory for Modification of Chemical Fibers and Polymer Materials, Donghua University, Shanghai 201620, People's Republic of China
[b]College of Chemistry, Chemical Engineering and Biotechnology, Donghua University, Shanghai 201620, People's Republic of China. E-mail: hcl@dhu.edu.cn
[c]College of Materials Science and Engineering, Donghua University, Shanghai 201620, People's Republic of China

or degradation-controlled depending on the polymer and the electrospinning approach used. Although these approaches provide multiple release profiles for the resultant fiber mats, there are still certain limitations in their use.[18,19] To overcome these limitations, some nanoscale carriers such as mesoporous silica nanoparticles (MSNs),[20,21] hydroxyapatite,[12] and liposome[22] have recently been incorporated into electrospun nanofibers for potential anticancer therapy, from which the prolonged drug release with tunable drug release kinetics could be achieved, and therefore provide particular benefit for postsurgical cancer treatment. MSNs have recently emerged as promising drug delivery carriers because of their good biocompatibility, large specific surface area, tunable mesoporous structure, and facile surface functionalization.[23–25] Moreover, MSNs could enhance the dissolution of the poorly water-soluble drugs and increase their bioavailability,[26] and MSNs with small sizes preferably accumulate at tumor sites caused by the enhanced permeability and retention (EPR) effect.[27,28] As a result, they have been widely employed for a variety of biomedical applications and especially for cancer diagnosis and therapy. Although previous studies[20,21] have reported that MSNs-embedded electrospun fiber mats could co-deliver two model fluorescent dyes in well-controlled release kinetics, the development of such a drug delivery system for postsurgical cancer treatment has been rarely reported.

We have previously shown that electrospun poly(L-lactide) (PLLA) nanofibers could be effectively used as carriers for antibiotic delivery[18,29] and scaffolds for tissue engineering.[30,31] We hypothesized that incorporation of anticancer drug-loaded MSNs into electrospun PLLA nanofibers would provide additional advantages for the treatment of a tissue defect after tumor resection. As a proof of concept, herein we report the development of an implantable MSNs-embedded nanofibrous scaffold for potential postsurgical cancer treatment. MSNs were synthesized and used as carriers for encapsulation of the anticancer drug doxorubicin hydrochloride (DOX), DOX-loaded MSNs (DOX@MSNs) were then embedded in PLLA nanofiber mats using electrospinning. The physicochemical properties, drug entrapment, and *in vitro* drug release of DOX-loaded nanofiber mats (PLLA/DOX@MSNs) were investigated. The potential use of these nanofiber mats for postsurgical cancer treatment were evaluated *in vitro* against cancerous HeLa cells.

Experimental

Materials

PLLA with a weight-average molecular weight (M_w) of 247 000 g mol^{-1} was obtained from Daigang Biomaterials Inc. (Jinan, China) and purified by dissolving in chloroform and recrystallization in ethanol. DOX was purchased from Beijing HuaFeng United Technology Co., Ltd. Proteinase K, tetraethylorthosilicate (TEOS), and cetyltrimethylammonium bromide (CTAB) were purchased from Sigma-Aldrich (Shanghai) Trading Co., Ltd. (Shanghai, China). All other chemicals were of analytical grade and obtained from Sino-pharm Chemical Reagents Co., Ltd. (Shanghai, China). HeLa cells were supplied by Institute of Biochemistry and Cell Biology (the Chinese Academy of Sciences, Shanghai, China). Dulbecco's Modified Eagle's Medium (DMEM), fetal bovine serum (FBS), 3-(4,5-dimethylthiazol-2-yl)-2,5-diphenyltetrazoliumbromide (MTT), trypsin, penicillin (100 U mL^{-1}) and streptomycin (100 μg mL^{-1}) were all purchased from Shanghai Yuanxiang medical equipment Co., Ltd. 4′,6-Diamidino-2-phenylindole (DAPI) was obtained from Byeotime Institute of Biotechnology (Jiangsu, China). Alexa Fluor@ 488 phalloidin was obtained from Invitrogen Trading Co., Ltd. (Shanghai, China).

Preparation of DOX@MSNs

MSNs were synthesized using the surfactant templating method and the template (CTAB) was finally removed from MSNs by the acidic extraction method.[32] Briefly, CTAB was dissolved in 500 mL buffer solution (pH 7.0) containing 3.43 g KH_2PO_4 and 0.58 g NaOH at 25 °C. Then TEOS was added dropwise to the mixed solution under vigorous stirring and the mixture was aged for 20 h. The synthesized samples were filtered through a filter of 0.22 μm, washed with double-distilled water and ethanol for three times, and air-dried at room temperature. The mixture samples were refluxed three times in the solution containing 300 mL ethanol and 4 mL hydrochloric acid at 78 °C for 8 h, then filtered and washed with ethanol. Finally, MSNs were obtained by drying in the drying oven at 80 °C.

A modified vacuum nano-casting route was applied to load DOX into MSNs as previously reported.[33] Briefly, DOX solution was firstly prepared as follows: 30 mg DOX was completely dissolved into 15 mL ethanol (100%), then refrigerated at −20 °C for 30 min to reduce ethanol volatilization in the following drug loading. The ethanol solution of DOX was added dropwise into 300 mg dry MSNs until full soakage, and the rest of the solution was kept frozen at −20 °C. Then the soaked nanoparticles were vacuumized slowly at room temperature for 30 min. The above-mentioned soakage–vacuum procedures were repeated until 15 mL of the ethanol solution of DOX was used up. To transfer the DOX molecules adsorbed on the external surface of MSNs into the pores, the nanoparticles were treated with three repeated cycles of washing with 1 mL ethanol and vacuum absorption. The obtained DOX@MSNs were vacuum-dried at room temperature for 12 h to a constant weight, followed by sealing and storing at −20 °C before further use. DOX loading efficiency was calculated as follows:

$$\text{Loading efficiency} = M_{DOX}/(M_{DOX} + M_{MSNs}) \times 100\%$$

where M_{DOX} and M_{MSNs} are the masses of the encapsulated DOX and MSNs, respectively.

Preparation of drug-loaded composite nanofibers

The prepared DOX@MSNs nanoparticles were subsequently incorporated into PLLA nanofibers using a blend electrospinning, and the nanofibers thus prepared are denoted as PLLA/DOX@MSNs. The DOX contents in PLLA/DOX@MSNs composite nanofibers were 0.5%, 1.0% and 1.5%, thus the corresponding MSNs contents in nanofibers can be calculated from the loading efficiency of MSNs. The PLLA/DOX composite

nanofibers were also prepared by electrospinning of PLLA/DOX blend solutions for comparison of their drug release profiles and cytotoxicity. In a typical procedure, PLLA was dissolved in a mixture of methylene chloride and dimethyl formamide (9 : 1, v/v) at 10% concentration (w/v). DOX@MSNs or neat DOX was added into the PLLA solution and stirred thoroughly to form a homogenous blend for subsequent electrospinning. The solution was filled into a 2.5 mL plastic syringe with an 18 gauge blunt-ended needle, and the distance between the needle and the aluminum foil collector was 15 cm. The syringe was loaded in a syringe pump (789100C, Cole-Parmer Instruments, USA) and dispensed at a rate of 1 mL h^{-1} at the applied voltage of 10 kV using a high voltage power supply (BGG6-358, BMEICO. Ltd. China). The collected nanofibers were vacuum dried at least 72 h to remove the residual solvent before further use.

Characterization

The surface morphologies of the MSNs and electrospun mats were observed by a field emission scanning electron microscope (FESEM, Hitachi S-4800, Japan) and a scanning electron microscope (SEM, Hitachi TM-1000, Japan). Before FESEM observation, MSNs were dispersed in ethanol, placed a drop onto a silica wafer. After drying, MSNs onto the silica wafer were sputter coated with gold films and observed with FESEM. As for SEM observation of electrospun mats, the nanofibers were also sputter coated with gold films. The distribution of MSNs in the nanofibers was observed by a transmission electron microscope (TEM, Hitachi H-800, Japan) at an operating voltage of 200 kV. Nanofibers for TEM were loaded onto a copper/carbon grid and air-dried before measurement. The particle size distribution of MSNs was determined by dynamic light scattering (DLS) measurements using a Malvern Zetasizer Nano ZS model ZEN3600 (Worcestershire, UK) equipped with a standard 633 nm laser. The zeta potential of the nanoparticles was also measured on a Zetasizer Nano ZS apparatus (Malvern, UK). The average diameter of nanofibers was obtained from at least 50 measurements on a typical FESEM image using Image J 1.40 G software (NIH, USA). The fluorescent images of PLLA/DOX and PLLA/DOX@MSNs composite nanofibers were observed by a fluorescence microscope (Nikon TS100, Japan). For analysis, the nanofibers were loaded onto the glass slide during the process of the electrospinning.

Nitrogen adsorption–desorption isotherms were measured with a Micromeritics Tristar II analyzer (Micromeritics, USA) at liquid nitrogen temperature under a continuous adsorption condition, MSNs were outgassed at 100 °C for at least 12 h before measurements. Average pore size distributions of MSNs were determined from the desorption branches of isotherms by the Barrett–Joyner–Halenda (BJH) method and the specific surface area was calculated according to the Brunauer–Emmett–Teller (BET) method. Attenuated total reflection Fourier transform infrared spectroscopy (ATR-FTIR) was performed by a Nicolet-670 FTIR spectrometer (Nicolet-Thermo, USA). All spectra were measured in the wavelength range of 500 to 4000 cm^{-1} with a resolution of 4 cm^{-1}. X-ray diffraction (XRD) patterns were obtained with a D/max-2500 PC diffractometer (Rigaku Co., Japan) using Cu/K_α radiation with a wavelength of 0.154 nm at 40 kV and 200 mA over the range of 5–60°. The thermogravimetric analysis (TGA) was employed to evaluate the weight loss of the samples in air from the room temperature to 900 °C at a heating rate of 10 °C min^{-1} using a thermal analyzer (TG 209 F1, Germany).

The tensile testing of the composite nanofibers was performed using a universal material tester (H5K-S, Hounsfield, U.K.) with a 50 N load cell under ambient conditions. A straight-line sample with a planar area of 50 mm × 10 mm was cut for tensile testing, as described in our previous work.[31] A cross-head speed of 10 mm min^{-1} was used for all the specimens. At least 5 specimens were tested for each group.

In vitro drug release

The DOX release behaviors of the PLLA/DOX@MSNs composite nanofibers were investigated with proteinase K in PBS at pH 7.4. For comparison, PLLA/DOX composite nanofibers containing the same DOX contents were also investigated for reference. The blank PLLA/MSNs and PLLA nanofibers with the same concentration as the experimental groups were used as controls to eliminate potential interference by enzyme and MSNs. Briefly, a piece of composite nanofibrous mat (80 mg, DOX were about 0.8 and 1.2 mg for PLLA/1.0% DOX@10% MSNs and PLLA/1.5% DOX@15% MSNs nanofibers respectively) was soaked in a centrifuge tube filled with 15 mL of PBS (pH 7.4) containing 50 μg mL^{-1} proteinase K. The centrifuge tube was incubated at 37 °C in a thermostatted shaker with the shaking speed of 100 rpm. At selected time intervals, 3 mL of the release medium was taken out and replaced with an equal volume of fresh PBS containing proteinase K. The collected release medium was filtered through a filter of 0.22 μm and then monitored by a Jasco V530 UV-Vis spectrophotometer (Jasco, Japan) at a wavelength of 480 nm. The absorbance was converted to its concentration according to the calibration curve of DOX in the same buffer solution. The content of DOX was determined as the average value of three parallel samples. The total contents of DOX in both medicated nanofibrous mats were determined using the same detection procedure as given above except that different release media were used. For the PLLA/DOX mat, the total content of DOX was measured after the nanofibrous mat (80 mg) was degraded completely in 15 mL of PBS (pH 7.4) containing 100 μg mL^{-1} of proteinase K. The same degradation procedure was carried out for the PLLA/DOX@MSNs mat, but an adequate volume of hydrofluoric acid (HF) was subsequently added to adjust the pH to 1.0 for fully dissolving all the MSNs in the solution.

Cytotoxicity assay of DOX-loaded composite nanofibrous mats

HeLa cells were cultured in the DMEM medium supplemented with 10% FBS, 100 U mL^{-1} penicillin and 100 μg mL^{-1} streptomycin. The cells were cultured at 37 °C in a humidified atmosphere containing 5% CO_2. For all experiments, cells were harvested by using trypsin solution and resuspended in the fresh DMEM medium. Prior to cell seeding, the electrospun

nanofibers were sterilized under UV light for 3 h and washed with PBS for three times.

The cytotoxicity of PLLA/DOX@MSNs composite nanofibers against HeLa cells was evaluated by the MTT assay after treatment of cells with electrospun nanofibers, and the cytotoxicity of bare MSNs (the same amount as that used in nanofibers), neat PLLA nanofibers and PLLA/DOX nanofibers with the equivalent of DOX was also tested for comparison. Briefly, HeLa cells (1×10^4 cells per well) were seeded in 24-well plates and incubated overnight at 37 °C to allow cells to attach. Then the medium was changed with a fresh medium (negative control) and the medium containing the MSNs, PLLA, free DOX (positive control), PLLA/1.0% DOX and PLLA/1.0% DOX@10% MSNs composite nanofibers at the total DOX concentrations of 10 μg mL^{-1}, 25 μg mL^{-1} and 50 μg mL^{-1} for 24 h, 48 h and 72 h. After a predetermined time point, the culture medium was removed and the cultured cells were washed twice with PBS. Then 360 μL of the fresh culture medium and 40 μL of MTT solution (5 mg mL^{-1} in PBS) were added to each well and incubation was continued for another 4 h. After removing the 400 μL suspension, 400 μL of DMSO was added to each well to solubilize the precipitate. Then 100 μL of the resulting supernatant was transferred to 96-well microplates and the absorbance was measured by a microplate reader (MK3, Thermo, USA) at the wavelength of 492 nm. The relative cell viability was calculated by $[OD]_{test}/[OD]_{control} \times 100\%$, and the average value was obtained from five parallel samples.

The morphologies of HeLa cells treated with PLLA, MSNs, PLLA/1.0% DOX, PLLA/1.0% DOX@10% MSNs composite nanofibers and free DOX at the total DOX concentration of 25 μg mL^{-1} for 24 h and 72 h were analyzed using SEM (JSM-5600 LV, JEOL, Japan) and confocal laser scanning microscopy (CLSM, Carl Zeiss LSM 700, Germany).

For SEM observation, the cells were washed with PBS and fixed with 2.5% glutaraldehyde in PBS buffer for 4 h. Then the fixed samples were dehydrated in an ascending series of ethanol (15%, 50%, 75%, 80%, 90% and 100%) for 20 min each and dried in a vacuum. Afterwards, the samples were sputter coated with gold and observed by SEM at an accelerating voltage of 15 kV. For confocal microscopy observation, HeLa cells were washed with PBS and then fixed with 4% glutaraldehyde for 10 min at 4 °C. Thereafter, the cells were washed twice with PBS, and permeabilized in 0.1% Triton X-100 in PBS for 5 min, followed by blocking with 1% BSA for 20 min. After washing with PBS, the fixed cells were stained with Alexa Fluor@ 488 phalloidin solution (165 nM) for 10 min. For nucleus labeling, the cells were washed again with PBS, and stained with DAPI solution (100 nM) for 5 min. Then the samples were washed with PBS and observed by CLSM.

Statistical analysis

All experiments were conducted at least three times and all values were reported as the mean and standard deviation. Statistical analysis was carried out by the one-way analysis of variance (one-way ANOVA) and the Scheffe's post hoc test. The criteria for statistical significance were $*p < 0.05$ and $**p < 0.01$.

Results and discussion

The brief fabrication process of PLLA/DOX@MSNs composite nanofibers is shown in Fig. 1. MSNs were synthesized as reported elsewhere,[32] DOX was then loaded into MSNs. After that, the prepared DOX@MSNs were added into PLLA solution to fabricate PLLA/DOX@MSNs composite nanofibers by electrospinning. Based on the weight change of MSNs before and after DOX loading, the DOX loading efficiency in MSNs was calculated to be 9.09%. Therefore, the MSNs contents in PLLA/DOX@MSNs composite nanofibers were respectively 5%, 10% and 15% for predetermined DOX contents of 0.5%, 1.0% and 1.5%. For convenience, the obtained electrospun mats were denoted as PLLA/0.5% DOX@5% MSNs, PLLA/1.0% DOX@10% MSNs, and PLLA/1.5% DOX@15% MSNs, respectively.

The morphology and structure of MSNs

The morphology and structure of MSNs were analyzed by FESEM, TEM, DLS and nitrogen adsorption–desorption isotherm analysis. As seen from Fig. 2A and C, MSNs have a spherical shape and uniform particle size, with the mean hydrodynamic size of 110.19 nm measured by DLS (Fig. 2C). The polydispersity index (PDI) of nanoparticles was 0.18, indicating a relatively narrow particle size distribution, while the zeta potential of MSNs was -10.88 ± 3.39 mV due to the existence of silanol groups on MSNs. The wormlike pore structure and highly ordered mesoporous channels of MSNs were also clearly observed (Fig. 2B). The nitrogen adsorption–desorption isotherms and pore size distribution data of MSNs are shown in Fig. 2D, which exhibited the characteristic of mesoporous materials.[34] The specific surface area of MSNs was 909.97 m^2 g^{-1}, and the pore size distribution (inset) revealed that the average pore size was 3.5 nm. These results indicated that the synthesized silica nanoparticles possessed a reasonably small size for incorporating into polymer nanofibers and a large internal volume for drug loading.

Characterization of PLLA/DOX@MSNs composite nanofibers

The content of MSNs in the polymer is an important factor in electrospinning, which can affect the morphology and the diameter of the resulting nanofibers. From Fig. 3A–D, it can be seen that the surface morphologies of nanofibers became irregular, and the fiber diameters got more widely distributed

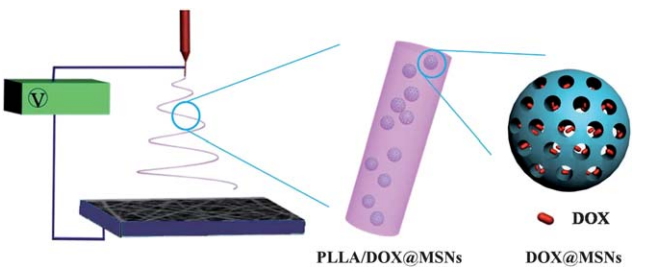

Fig. 1 Schematic illustration for the process of fabrication of PLLA/DOX@MSNs electrospun composite nanofibers and the location of DOX in the fiber.

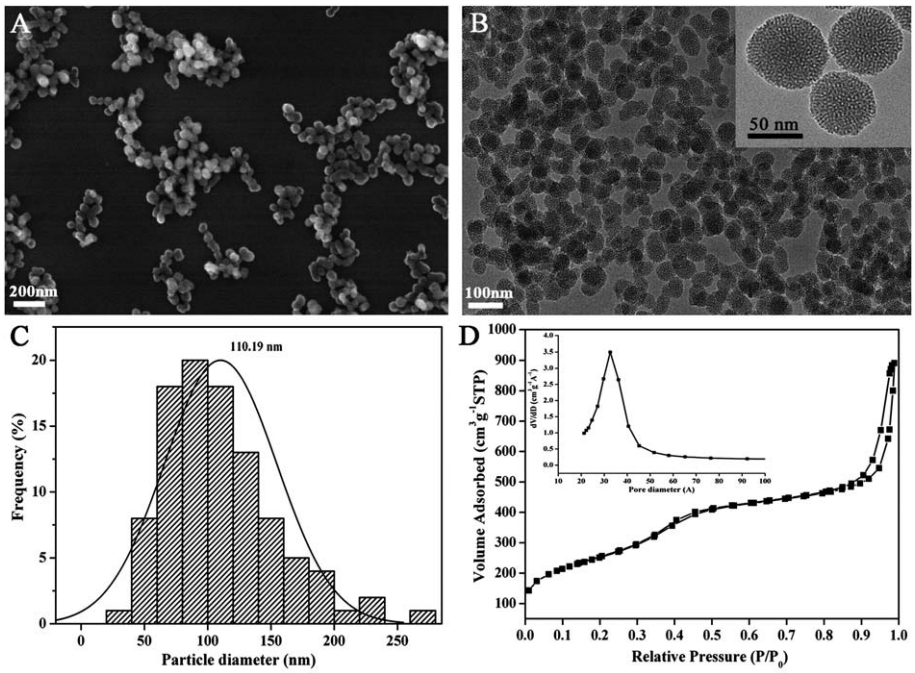

Fig. 2 The morphology, size distribution and structure of MSNs. (A) FESEM image, (B) TEM image (inset is the magnified image), (C) size distribution and (D) nitrogen adsorption–desorption isotherms (inset is pore size distribution) of MSNs.

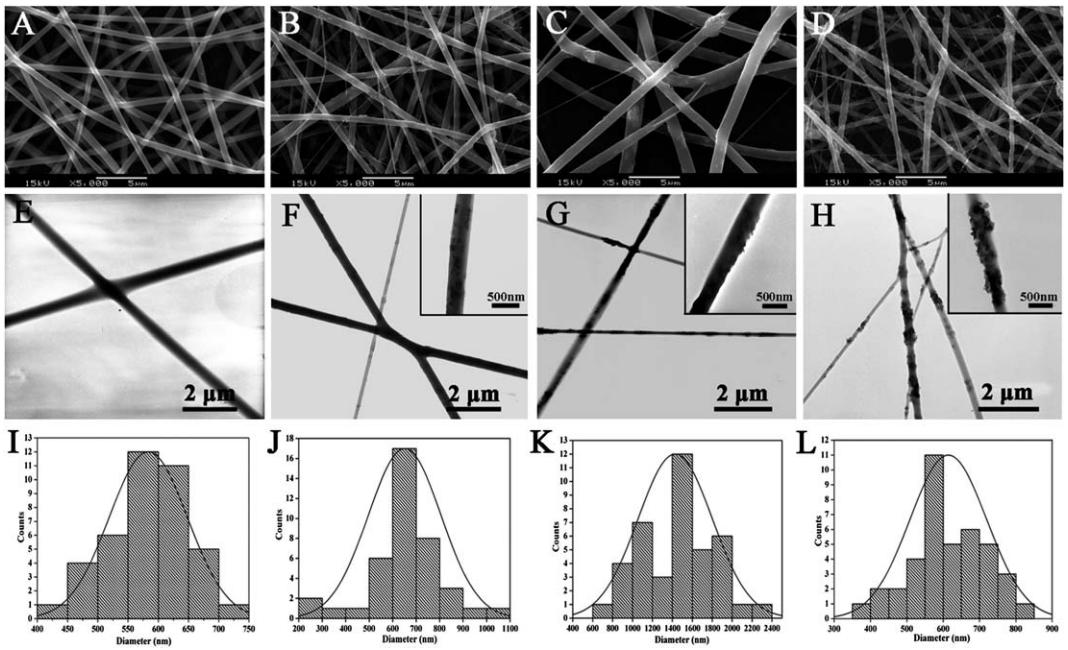

Fig. 3 The morphology and diameter distribution of PLLA and PLLA/DOX@MSNs composite nanofibers. SEM images of (A) neat PLLA, (B) PLLA/0.5% DOX@5% MSNs, (C) PLLA/1.0% DOX@10% MSNs, (D) PLLA/1.5% DOX@15% MSNs nanofibers. (E–H): the corresponding TEM images of (A)–(D) (insets are the magnified images). (I–L): the corresponding diameter distributions of (A)–(D).

with the increase of the MSNs content. In particular, when the content of MSNs was 15%, the surface morphologies of composite nanofibers got rough, with lots of protrusions being clearly observed on the surface of nanofibers. TEM images shown in Fig. 3E–H indicate the structure of DOX@MSNs-contained PLLA nanofibers, where MSNs formed a uniform dispersion in nanofibers when the MSNs content in the composite nanofibers was lower than 15%. However, the MSNs agglomeration could be observed when the MSNs content was up to 15%, which was consistent with the results obtained by Song *et al.*[21] From the SEM and TEM images, it can be observed that DOX@MSNs were positioned near the outer surface of the

fibers. In addition, the average diameter of the PLLA/MSNs fibers with 5% MSNs (651 ± 153 nm), 10% MSNs (1439 ± 394 nm), 15% MSNs (595 ± 123 nm) were all greater than neat PLLA nanofibers (583 ± 65 nm) (Fig. 3I–L). This phenomenon may be due to the increase in viscosity of the mixed solution with the content of MSNs increasing.[35] Hence, the optimal concentrations of MSNs were 5% and 10% which facilitate achieving composite nanofibers with homogenously dispersed MSNs.

The chemical structures of different nanofibers were evaluated using FTIR analysis. Fig. 4A shows the FTIR spectra of the MSNs, DOX, PLLA and PLLA/1.0% DOX@10% MSNs composite nanofibers. From the spectrum of MSNs, the peaks at 795 and 953 cm^{-1} can be assigned to the Si–O–Si and Si–OH stretching vibrations of MSNs, respectively, and the broad peak near 3468 cm^{-1} is associated with the intra- and intermolecular-hydrogen bonds of Si–OH groups.[36] From the FTIR spectra of the neat PLLA and PLLA/1.0% DOX@10% MSNs nanofibers, the absorption peaks at approximately 1757 and 1188 cm^{-1} can be attributed to C═O stretching and C–O–C stretching of PLLA, respectively.[31] However, no characteristic absorption peaks of MSNs and DOX (the typical absorption bands at 1088, 1285, 1434 and 1621 cm^{-1}) can be observed in the spectrum of PLLA/1.0% DOX@10% MSNs nanofibers, which may be caused by the fact that DOX@MSNs were effectively embedded into the interior of the composite nanofibers.

XRD patterns of MSNs, PLLA, and PLLA/DOX@MSNs composite nanofibers were shown in Fig. 4B. A broad peak centered at $2\theta = 23°$ related to the amorphous SiO_2 was observed in the XRD pattern of MSNs, which was consistent with the results of previous studies.[37,38] Furthermore, electrospun PLLA nanofibers only displayed a broad and diffuse diffraction peak at 2θ of 21°, which indicated that PLLA was amorphous. However, from XRD patterns of various PLLA/DOX@MSNs nanofibers, the peak at $2\theta = 15°$ became sharper with increasing MSNs content in PLLA nanofibers, which confirmed that the addition of MSNs could improve the crystallinity of nanofibers.[39]

TGA was used to examine the thermal properties of the prepared PLLA/DOX@MSNs composite nanofibers. As shown in Fig. 4C, a moderate decrease in weight before 100 °C could be due to the vaporization of water in nanofibers. The weight decreased rapidly from approximately 250 °C to 400 °C, which can be attributed to the strong decomposition of PLLA and DOX. From curves in Fig. 4C, it can be observed that the weight percentages of residual MSNs were 4.2%, 9.0% and 12.2% for composite nanofibers with 5%, 10% and 15% of MSNs content, respectively, which are almost equal to the initially added weight of MSNs. Therefore, MSNs could be incorporated into the nanofibers with less weight loss during the electrospinning process. The TGA curves also indicated the effect of different MSN contents on the thermal stability of composite nanofibers.

Table 1 Tensile mechanical properties of PLLA nanofibers and PLLA/DOX@MSNs nanofibers

MSNs content (%)	Tensile strength (MPa)	Elongation at break (%)	Young's modulus (MPa)
0	6.64 ± 0.94	122.02 ± 34.20	163.71 ± 3.30
5	2.97 ± 0.70	66.29 ± 13.62	81.13 ± 8.67
10	1.42 ± 0.23	59.58 ± 2.10	26.35 ± 2.56
15	1.22 ± 0.17	25.25 ± 3.91	20.33 ± 2.37

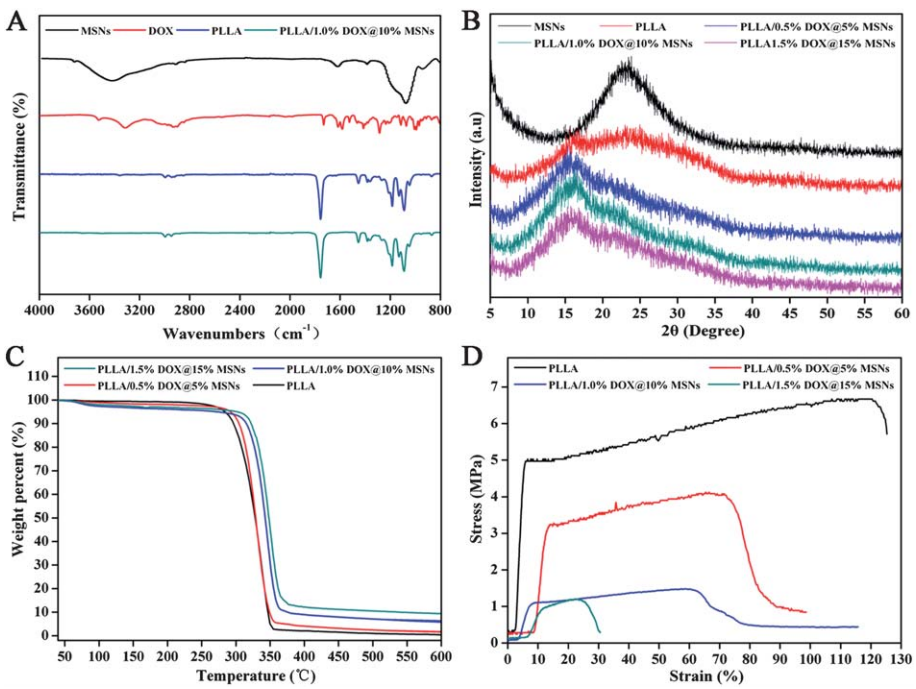

Fig. 4 Characterization of PLLA and PLLA/DOX@MSNs. (A) ATR-FTIR spectra. (B) XRD patterns. (C) TGA thermograms. (D) Typical tensile stress–strain curves.

The onset degradation temperature (T_{onset}) of the PLLA sample was 307.4 °C, whereas all composite samples showed prominent increase in the T_{onset} value, suggesting that the addition of MSNs can improve the thermal stability of the composites.

The typical tensile strain–stress curves of neat PLLA and the PLLA/DOX@MSNs composite nanofibers with different MSNs contents are shown in Fig. 4D, and the mechanical properties of PLLA/DOX@MSNs composite nanofibers are summarized in Table 1. It can be found that the tensile strength decreased with the increase of MSNs contents, which was basically in agreement with the data of the elongation at break and the Young's modulus. For example, the elongation at break for composite

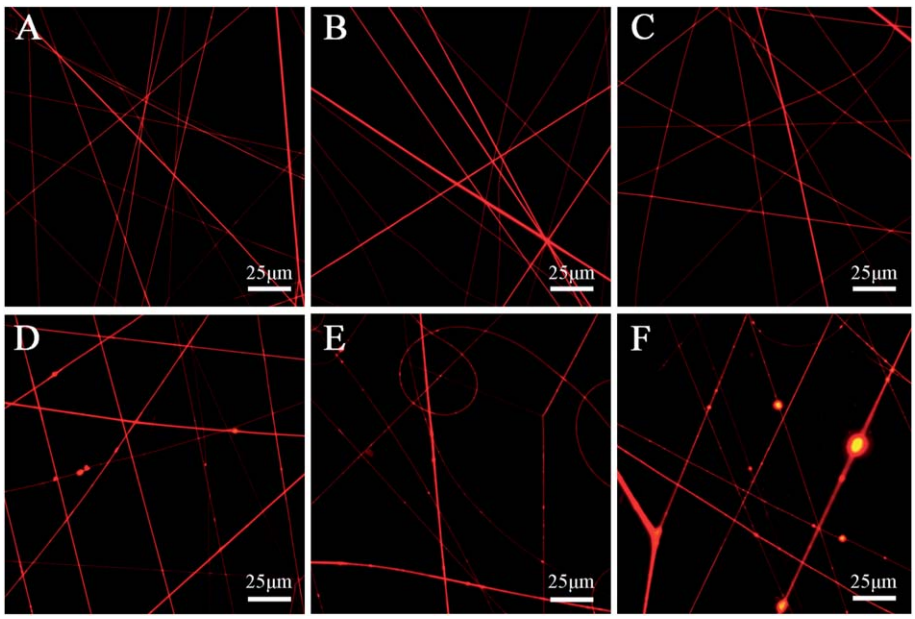

Fig. 5 Fluorescent images of PLLA/DOX and PLLA/DOX@MSNs composite nanofibers. (A) PLLA/0.5% DOX, (B) PLLA/1.0% DOX, (C) PLLA/1.5% DOX, (D) PLLA/0.5% DOX@5% MSNs, (E) PLLA/1.0% DOX@10% MSNs and (F) PLLA/1.5% DOX@15% MSNs composite fibers.

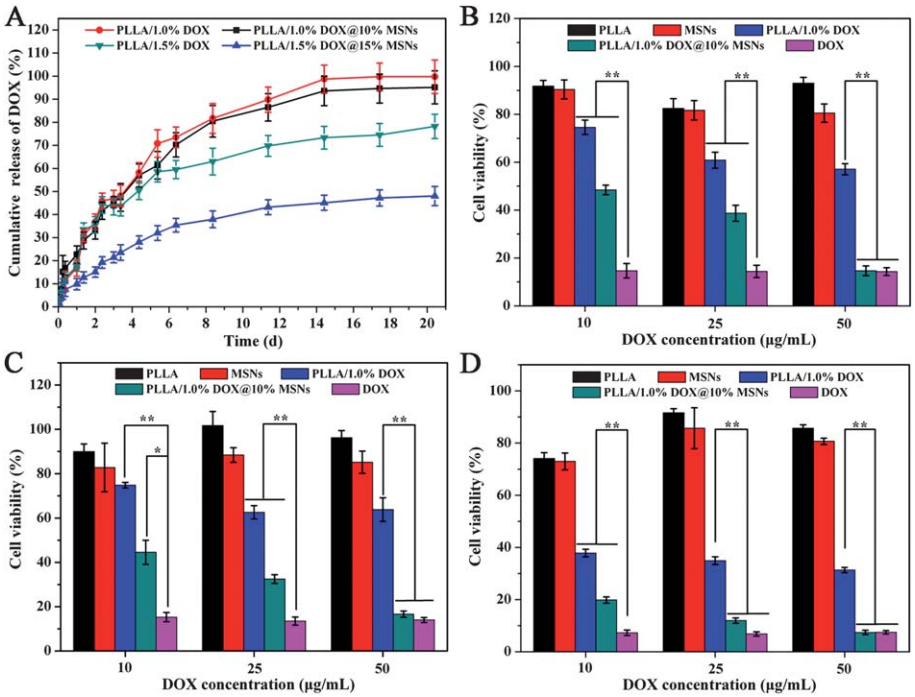

Fig. 6 (A) The cumulative DOX release profiles from various nanofibrous mats. Cell viability of HeLa cells treated with different samples with DOX concentrations ranging from 10 to 50 μg mL^{-1} for (B) 24 h, (C) 48 h and (D) 72 h. Significant difference between groups is indicated (*$p < 0.05$; **$p < 0.01$).

nanofibers with 15% of MSNs content was only 25.3% as compared to 122.0% for neat PLLA nanofibers. The result can be supported by the TEM and SEM images in Fig. 3D and H, where MSNs aggregation can be observed, which would destroy the original structure of nanofibers due to the poor interfacial adhesion between the MSNs and the PLLA matrix, and thus reduces the mechanical properties of the composite structure.

DOX loading and release profiles

For comparison, the PLLA/DOX electrospun mats containing the equivalent DOX contents with PLLA/DOX@MSNs electrospun mats were also prepared for the following drug release and *in vitro* cytotoxicity studies. Accordingly, these electrospun mats are denoted as PLLA/0.5% DOX, PLLA/1.0% DOX and PLLA/1.5% DOX, respectively.

The DOX loaded in composite nanofibers can be clearly observed by the red fluorescence of DOX using a fluorescence microscope (Fig. 5). All the PLLA/DOX composite nanofibers exhibited a uniform red fluorescence (Fig. 5A–C), which is attributed to homogeneous dispersion of DOX in the nanofibers. In contrast, the PLLA/DOX@MSNs composite nanofibers showed a local stronger red fluorescence as compared to their PLLA/DOX counterparts (Fig. 5D–F), this may have been caused by the partial aggregation of nanoparticles in the nanofibers.

PLLA is a semicrystalline polyester with high crystallinity and hydrophobicity, which make it degrade very slowly both *in vitro* and *in vivo*.[31] The use of proteinase K to accelerate the degradation of PLLA, therefore, has been considered as an effective approach in obtaining overall drug release profiles of PLLA-based drug delivery systems in a very short time period.[13,14,16] The electrospun mats containing 1.0% and 1.5% DOX contents were selected for comparative drug release studies, because previous studies have shown that the sustained DOX release and effective anticancer cytotoxicity could be achieved when DOX content in electrospun mats was up to 1.0%.[12,15] Fig. 6A

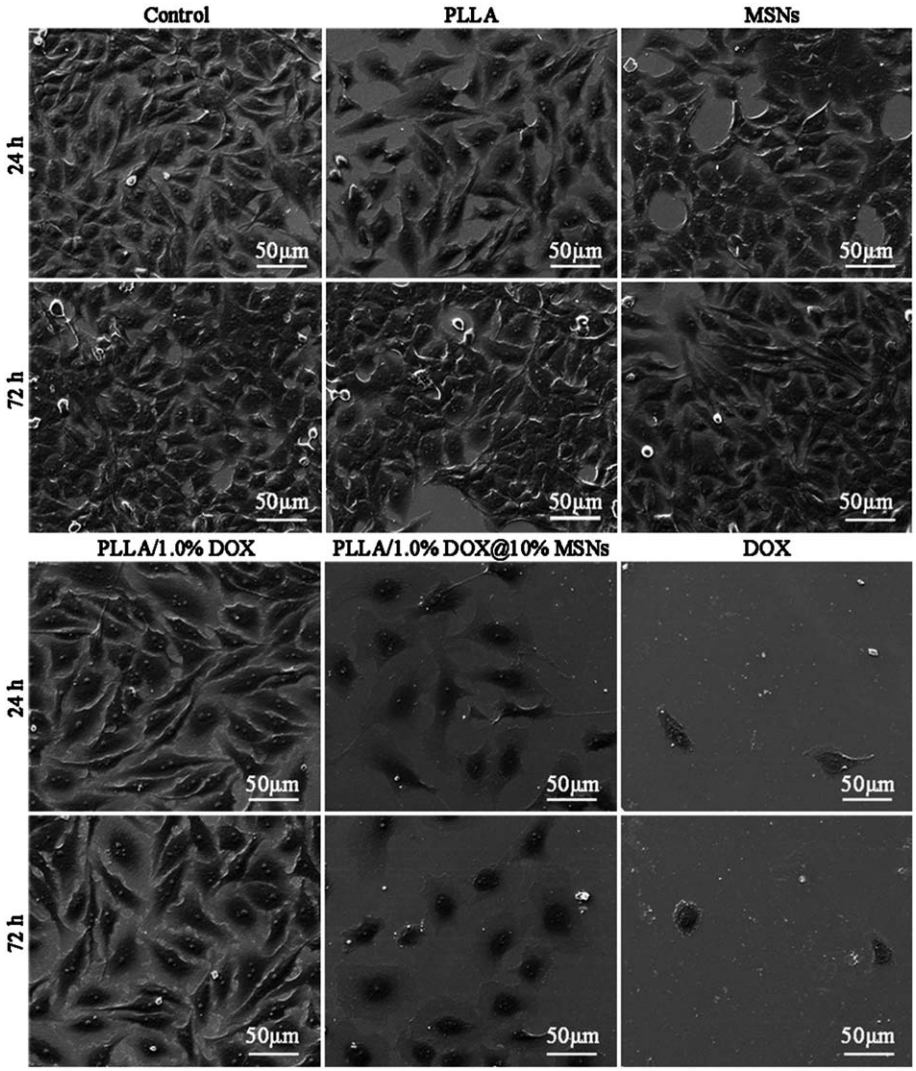

Fig. 7 SEM micrographs of HeLa cells treated with PLLA, PLLA/1.0% DOX, MSNs, PLLA/1.0% DOX@10% MSNs and free DOX for 24 h and 72 h. DOX concentration was 25 μg mL^{-1}.

shows the release profiles from 1.0% and 1.5% DOX-loaded electrospun mats. All the electrospun mats, except for the PLLA/1.5% DOX@15% MSNs nanofibers, indicated a similar two-stage release behavior, an initial rapid release followed by a constant release during 20 days of incubation. For example, over 40% of DOX was released from PLLA/1.0% DOX, PLLA/1.0% DOX@10% MSNs and PLLA/1.5% DOX mats at 60 h. In contrast, only 19.2% of DOX was released from the PLLA/1.5% DOX@15% MSNs mats at the same time period. The initial rapid release is mainly due to the DOX molecules distributed close to the fibers surface during the electrospinning process. Interestingly, the release rate of DOX for both nanofiber formulations (with and without MSNs) decreased with increasing DOX content in the fibers during the whole drug release period, and the MSNs-containing formulations contributed a more steady drug release profile compared to their MSNs-free counterparts. These results indicate that MSNs-containing electrospun mats could be tailored to provide an initial rapid release followed by a sustained release of the drug. An initial rapid drug release is preferable for inhibition of the tumor cell growth by providing sufficient initial dosage of the anticancer drug within a short time period, and the subsequent sustained release allows us to maintain a desired therapeutic concentration of anticancer drug over an extended period of time, which is very beneficial for preventing the proliferation of the cancer cells that survive the initial stage of the drug release.[15,40,41]

In vitro cytotoxicity effect on HeLa cells

To verify pharmacological efficacy of the released DOX, the cytotoxicity of the composite nanofibers with different DOX contents against HeLa cells was evaluated by the MTT assay. According to the release rate of DOX from both nanofiber formulations, the electrospun mats with 1.0% DOX loading (PLLA/1.0% DOX@10% MSNs and PLLA/1.0% DOX) were selected as the representative to evaluate their cytotoxicity.

HeLa cells were treated with different samples for 24 h, 48 h and 72 h. As shown in Fig. 6B–D, in the case of neat PLLA nanofibers and bare MSNs, they did not display any obvious

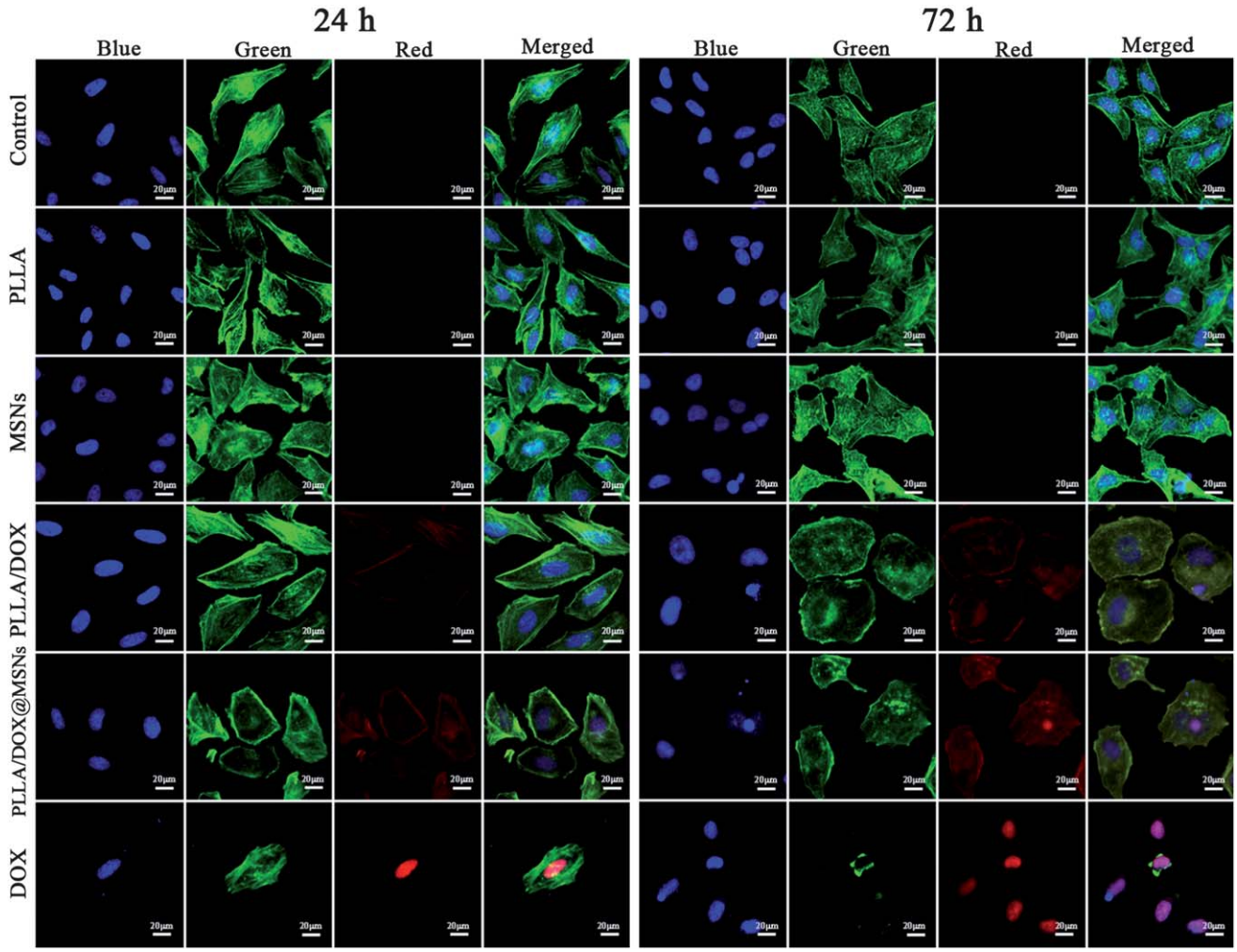

Fig. 8 Confocal laser scanning microscopy images of HeLa cells treated with PLLA, PLLA/1.0% DOX, MSNs, PLLA/1.0% DOX@10% MSNs and free DOX for 24 h and 72 h. DOX concentration was 25 μg mL^{-1}. Blue, green and red fluorescence respectively represent the DAPI-stained cell nuclei, the Alexa Fluor@ 488 phalloidin-stained F-actin and the released DOX. The yellow and pink suggest the entry of the released DOX into the cytoplasm and the cell nuclei, respectively.

cytotoxicity to HeLa cells within the measured concentrations and time periods. The cytotoxicity of PLLA/1.0% DOX@10% MSNs, PLLA/1.0% DOX composite nanofibers and free DOX against HeLa cells increased with the increase of the total DOX concentration and the incubation time (Fig. 6B–D). However, the PLLA/1.0% DOX and PLLA/1.0% DOX@10% MSNs composite nanofibers showed a statistically significant lower inhibition effect than free DOX when the DOX concentration was less than 25 μg mL^{-1} from 24 h to 48 h. This is probably because a large proportion of DOX molecules was still within the composite nanofibers, which results in a lower DOX concentration in the medium of the composite nanofibers than that of free DOX. In contrast, when the total DOX concentration increased to 50 μg mL^{-1}, the cytotoxicity of PLLA/1.0% DOX@10% MSNs composite nanofibers was similar to free DOX, which was statistically significantly higher than that of PLLA/1.0% DOX nanofibers ($p < 0.01$), and the cell viability decreased from $14.67 \pm 2.02\%$ to $7.41 \pm 0.83\%$ from 24 h to 72 h of incubation. Therefore, DOX incorporated into MSNs-containing nanofibers seemed to have a higher cytotoxic effect on the HeLa cells than their MSN-free counterparts. Although the mechanism is not clear, the beneficial results from MSNs-containing nanofibers might be explained by reducing the adverse impact of the solvent and electric field on the antitumor activity of DOX, due to the protection provided by MSNs during the electrospinning process. It can be expected that a long-term growth inhibition in cancer cells could be achieved with the sustained DOX release from the MSNs-containing composite scaffold after the scaffold was implanted into the body.

The morphological changes of HeLa cells treated with different samples at the DOX concentration of 25 μg mL^{-1} for 24 h and 72 h were observed by SEM and CLSM. The SEM images in Fig. 7 show that HeLa cells adopt an extended morphology after treating with neat PLLA fibers and bare MSNs, which is similar to the control, indicating no toxicity of the neat PLLA nanofibers and MSNs under the conditions of this experiment. However, cells treated with both PLLA/1.0% DOX and PLLA/1.0% DOX@10% MSNs nanofibers acquired a round-shaped morphology and a reduced cell number compared to cells treated with neat PLLA nanofibers. Specifically, cells treated with PLLA/1.0% DOX@10% MSNs nanofibers for both time points exhibited apoptotic morphological changes, including cellular shrinkage and cytoplasmic vacuolization, which can be further confirmed by the CLSM images that the red fluorescence of DOX in the nucleus were clearly observed for PLLA/1.0% DOX@10% MSNs nanofibers (Fig. 8). The results suggest that DOX released from both the composite nanofibers is cytotoxic on HeLa cells. In addition, the SEM images (Fig. 7) showed that treatment of HeLa cells with free DOX caused rapid cellular apoptosis, and the merged confocal images (Fig. 8) indicated that free DOX could enter into HeLa cells and accumulate in the nucleus after 24 h of incubation. Taking all the results together, we can expect that the MSNs-containing composite nanofibers would exhibit efficient and long-term antitumor efficacy, which might be used as a potential implantable device for the prevention of cancer recurrence, by surgical implantation into the site or cavity area where a tumor was resected.

Conclusions

In summary, various PLLA/DOX@MSNs composite nanofibers were successfully fabricated *via* electrospinning. The resultant composite nanofibers might be potentially used as implantable scaffolds for postsurgical cancer treatment. We showed that the PLLA/1.0% DOX@10% MSNs composite nanofibers not only provide a good particle distribution in nanofibers and an improved thermal stability, but also possess high DOX-loading capacities, from which the drug can be released in a sustained and prolonged manner, and therefore higher *in vitro* antitumor efficacy than their MSNs-free counterparts. Thus, the prepared PLLA/MSNs composite nanofibers are highly promising as local implantable scaffolds for the treatment of a tissue defect after tumor resection.

Acknowledgements

This work was financially supported by the National Natural Science Foundation of China (31271028), Shanghai Natural Science Foundation (11ZR1400100), Shanghai Nano Science Program (11nm0505500), Innovation Program of Shanghai Municipal Education Commission (13ZZ051), Fundamental Research Funds for the Central Universities, Open Foundation of State Key Laboratory for Modification of Chemical Fibers and Polymer Materials (LK1202), Chinese Universities Scientific Fund (13D310608), and the Scientific Research Foundation for Returned Scholars, Ministry of Education of China.

Notes and references

1 J. B. Wolinsky, R. Liu, J. Walpole, L. R. Chirieac, Y. L. Colson and M. W. Grinstaff, *J. Controlled Release*, 2010, **144**, 280–287.
2 V. Gupta, G. H. Mun, B. N. Choi, A. Aseh, L. Mildred, A. Patel, Q. X. Zhang, J. E. Price, D. Chang, G. Robb and A. B. Mathur, *Ann. Biomed. Eng.*, 2011, **39**, 2374–2387.
3 J. W. Xie, R. S. Tan and C. H. Wang, *J. Biomed. Mater. Res., Part A*, 2008, **85**, 897–908.
4 S. T. Yohe, V. L. M. Herrera, Y. L. Colson and M. W. Grinstaff, *J. Controlled Release*, 2012, **162**, 92–101.
5 G. P. Ma, Y. Liu, C. Peng, D. W. Fang, B. J. He and J. Nie, *Carbohydr. Polym.*, 2011, **86**, 505–512.
6 X. M. Luo, C. Y. Xie, H. Wang, C. Y. Liu, S. L. Yan and X. H. Li, *Int. J. Pharm.*, 2012, **425**, 19–28.
7 R. Liu, J. B. Wolinsky, P. J. Catalano, L. R. Chirieac, A. J. Wagner, M. W. Grinstaff, Y. L. Colson and C. P. Raut, *Ann. Surg. Oncol.*, 2012, **19**, 199–206.
8 N. Lei, C. Y. Gong, Z. Y. Qian, F. Luo, C. Wang, H. L. Wang and Y. Q. Wei, *Nanoscale*, 2012, **4**, 5686–5693.
9 J. B. Wolinsky, Y. L. Colson and M. W. Grinstaff, *J. Controlled Release*, 2012, **159**, 14–26.
10 X. L. Xu, X. S. Chen, X. Y. Xu, T. C. Lu, X. Wang, L. X. Yang and X. B. Jing, *J. Controlled Release*, 2006, **114**, 307–316.
11 S. H. Ranganath and C. H. Wang, *Biomaterials*, 2008, **29**, 2996–3003.

12 F. Y. Zheng, S. G. Wang, M. W. Shen, M. F. Zhu and X. Y. Shi, *Polym. Chem.*, 2013, **4**, 933–941.
13 X. L. Xu, X. S. Chen, P. A. Ma, X. R. Wang and X. B. Jing, *Eur. J. Pharm. Biopharm.*, 2008, **70**, 165–170.
14 Z. Jing, X. Y. Xu, X. S. Chen, Q. Z. Liang, X. C. Bian, L. X. Yang and X. B. Jing, *J. Controlled Release*, 2003, **92**, 227–231.
15 M. G. Ignatova, N. E. Manolova, R. A. Toshkova, I. B. Rashkov, E. G. Gardeva, L. S. Yossifova and M. T. Alexandrov, *Biomacromolecules*, 2010, **11**, 1633–1645.
16 X. L. Xu, L. X. Yang, X. Y. Xu, X. Wang, X. S. Chen, Q. Z. Liang, J. Zeng and X. B. Jing, *J. Controlled Release*, 2005, **108**, 33–42.
17 S. J. Shao, L. Li, G. Yang, J. R. Li, C. Luo, T. Gong and S. B. Zhou, *Int. J. Pharm.*, 2011, **421**, 310–320.
18 C. L. He, Z. M. Huang and X. J. Han, *J. Biomed. Mater. Res., Part A*, 2009, **89**, 80–95.
19 A. Szentivanyi, T. Chakradeo, H. Zernetsch and B. Glasmacher, *Adv. Drug Delivery Rev.*, 2011, **63**, 209–220.
20 B. T. Song, C. T. Wu and J. Chang, *J. Biomed. Mater. Res., Part B*, 2012, **100**, 2178–2186.
21 B. T. Song, C. T. Wu and J. Chang, *Acta Biomater.*, 2012, **8**, 1901–1907.
22 A. Mickova, M. Buzgo, O. Benada, M. Rampichova, Z. Fisar, E. Filova, M. Tesarova, D. Lukas and E. Amler, *Biomacromolecules*, 2012, **13**, 952–962.
23 F. Q. Tang, L. L. Li and D. Chen, *Adv. Mater.*, 2012, **24**, 1504–1534.
24 P. P. Yang, S. L. Gai and J. Lin, *Chem. Soc. Rev.*, 2012, **41**, 3679–3698.
25 I. I. Slowing, J. L. Vivero-Escoto, C. W. Wu and V. S. Y. Lin, *Adv. Drug Delivery Rev.*, 2008, **60**, 1278–1288.
26 Y. Z. Zhang, Z. Z. Zhi, T. Y. Jiang, J. H. Zhang, Z. Y. Wang and S. L. Wang, *J. Controlled Release*, 2010, **145**, 257–263.
27 M. H. Yu, S. Jambhrunkar, P. Thorn, J. Z. Chen, W. Y. Gu and C. Z. Yu, *Nanoscale*, 2013, **5**, 178–183.
28 A. S. Hoffman, *J. Controlled Release*, 2008, **132**, 153–163.
29 C. L. He, Z. M. Huang, X. J. Han, L. Liu, H. S. Zhang and L. S. Chen, *J. Macromol. Sci., Part B: Phys.*, 2006, **45**, 515–524.
30 C. L. He, G. Y. Xiao, X. B. Jin, C. H. Sun and P. X. Ma, *Adv. Funct. Mater.*, 2010, **20**, 3568–3576.
31 C. L. He, W. Feng, L. J. Cao and L. P. Fan, *J. Biomed. Mater. Res., Part A*, 2011, **99**, 655–665.
32 Q. J. He, X. Z. Cui, F. M. Cui, L. M. Guo and J. L. Shi, *Microporous Mesoporous Mater.*, 2009, **117**, 609–616.
33 Q. J. He, J. M. Zhang, F. Chen, L. M. Guo, Z. Y. Zhu and J. L. Shi, *Biomaterials*, 2010, **31**, 7785–7796.
34 Y. J. Yang, X. Tao, Q. Hou and J. F. Chen, *Acta Biomater.*, 2009, **5**, 3488–3496.
35 M. Kanehata, B. Ding and S. Shiratori, *Nanotechnology*, 2007, **18**, 315602.
36 E. J. Lee, S. H. Teng, T. S. Jang, P. Wang, S. W. Yook, H. E. Kim and Y. H. Koh, *Acta Biomater.*, 2010, **6**, 3557–3565.
37 Z. Y. Hou, C. X. Li, P. A. Ma, Z. Y. Cheng, X. J. Li, X. Zhang, Y. L. Dai, D. M. Yang, H. Z. Lian and J. Lin, *Adv. Funct. Mater.*, 2012, **22**, 2713–2722.
38 A. Galarneau, J. Iapichella, K. Bonhomme, F. Di Renzo, P. Kooyman, Terasaki and F. Fajula, *Adv. Funct. Mater.*, 2006, **16**, 1657–1667.
39 A. A. Taha, Y. N. Wu, H. T. Wang and F. T. Li, *J. Environ. Manage.*, 2012, **112**, 10–16.
40 S. Liu, G. Y. Zhou, D. X. Liu, Z. G. Xie, Y. B. Huang, X. Wang, W. B. Wu and X. B. Jing, *J. Mater. Chem. B*, 2013, **1**, 101–109.
41 Y. Wang, P. P. Yang, P. A. Ma, F. Y. Qu, S. L. Gai, N. Niu, F. He and J. Lin, *J. Mater. Chem. B*, 2013, **1**, 2056–2065.